Modular DGTD Implementation for Doubly Dispersive Media With Curvilinear Elements

Tiago V. L. Amorim, Elson J. Silva, Fernando J. S. Moreira, *Senior Member, IEEE*, and Fernando L. Teixeira

***Abstract*—We present a novel modular implementation of the discontinuous Galerkin time-domain (DGTD) method to effectively address electromagnetic problems involving general doubly dispersive media. This approach includes an extended perfectly matched layer to directly truncate doubly dispersive materials, allowing for the modeling of open domains. The proposed modular and concise DGTD implementation, based on the complex-conjugate pole-residue model, offers flexibility and simplifies the handling of complex doubly dispersive medium problems with curvilinear boundaries. We apply the formulation to 2-D scattering problems, demonstrating very good agreement with their respective analytical solutions.**

***Index Terms*—Doubly dispersive media, scattering, discontinuous Galerkin time-domain (DGTD) method.**

I. Introduction

In recent years, the demand for advanced modeling techniques in electromagnetics has increased substantially, as driven, for example, by the need to accurately simulate complex materials with both electric and magnetic dispersive properties [1], [2].

In this work, we extend the modular implementation of the discontinuous Galerkin time-domain (DGTD) method [3] to account for 1) doubly dispersive media exhibiting both dielectric and magnetic dispersion effects and 2) grids with curvilinear elements [4], which enables more accurate modeling of complex geometries. The proposed DGTD formulation is also capable of tackling unbounded domains. While various methods have been proposed to handle unbounded domains, such as absorbing boundary conditions [5], [6] or integral equation-based approaches [7], this work implements an extension of the uniaxial perfectly matched layer (PML) technique [8] to general doubly dispersive media.

These advancements aim at extending the capability of the DGTD method to address a wider range of electromagnetic problems [9], [10], [11], particularly those involving dispersive materials [12], [13], [14], [15] with intricate shapes. The proposed algorithm is validated through several examples that demonstrate its robustness and versatility.

Received 24 February 2025; revised 29 April 2025 and 8 July 2025; accepted 9 August 2025. Date of publication 19 August 2025; date of current version 8 October 2025. This work was supported in part by CNPq and in part by CAPES-PROEX, Brazil. *(Corresponding author: Tiago V. L. Amorim.)*

Tiago V. L. Amorim is with the Graduate Program in Electrical Engineering, Federal University of Minas Gerais, Belo Horizonte 31270-901, Brazil (e-mail: tiagovla@ufmg.br).

Elson J. Silva is with the Department of Electrical Engineering, Federal University of Minas Gerais, Belo Horizonte 31270-901, Brazil (e-mail: elson@cpdee.ufmg.br).

Fernando J. S. Moreira is with the Department of Electronic Engineering, Federal University of Minas Gerais, Belo Horizonte 31270-901, Brazil (e-mail: fernandomoreira@ufmg.br).

Fernando L. Teixeira is with the ElectroScience Laboratory, The Ohio State University, Columbus, OH 43212 USA (e-mail: teixeira.5@osu.edu).

Digital Object Identifier 10.1109/LAWP.2025.3599788

II. Mathematical Formulation

A. Dispersive Media Modeling

In isotropic dispersive materials, the frequency-dependent permittivity can be expressed as $\epsilon(\omega) = \epsilon_0\epsilon_\infty + \epsilon_0\chi_e(\omega)$, where ϵ_∞ represents the high-frequency relative permittivity and $\chi_e(\omega)$ is the electric susceptibility. Following the complex-conjugate pole-residue (CCPR) model [16], $\chi_e(\omega)$ can be expanded as a sum of complex-conjugate pole pairs

$$\chi_e(\omega) = \sum_{r=1}^{R}\left(\frac{c_r}{j\omega - a_r} + \frac{c_r^*}{j\omega - a_r^*}\right) \tag{1}$$

where R is the number of poles, and a_r and c_r are the model's parameters that can be obtained from data fitting. The magnetic permeability $\mu(\omega)$ can sometimes exhibit a similar dispersive behavior, modeled as $\mu_0\mu_\infty + \mu_0\chi_m(\omega)$, where

$$\chi_m(\omega) = \sum_{s=1}^{S}\left(\frac{d_s}{j\omega - b_s} + \frac{d_s^*}{j\omega - b_s^*}\right) \tag{2}$$

with S poles and corresponding parameters b_s and d_s.

B. Generalized Doubly Dispersive Formulation

The generalized doubly dispersive formulation is derived from the uniaxial PML auxiliary differential equation approach [17] within the modular DGTD framework introduced in [3]. The CCPR model is used for its simplicity and natural compatibility with vector fitting techniques, although other general dispersive models could also be employed [18], [19], [20], [21]. By introducing dual-auxiliary fields, $\boldsymbol{\mathcal{S}}$ and $\boldsymbol{\mathcal{Q}}$, to account for magnetic dispersion, the full set of governing equations is presented in Fig. 1.

C. Discontinuous Galerkin Method

The DGTD method discretizes the spatial domain Ω_h into K nonoverlapping elements Ω_h^k, bounded by $\partial\Omega_h^k$, and approximates the solution using piecewise polynomial functions. This approach allows us to write the weak form of the generalized doubly dispersive formulation keeping the standard upwind numerical flux in bilinear form as

$$\epsilon_0\left(\phi_h, \epsilon_\infty\frac{\partial \boldsymbol{\mathcal{E}}_h}{\partial t}\right)_{\Omega_h} = (\phi_h, \nabla\times\boldsymbol{\mathcal{H}}_h)_{\Omega_h} + \epsilon_0(\phi_h, \boldsymbol{\mathcal{K}}_h)_{\Omega_h}$$

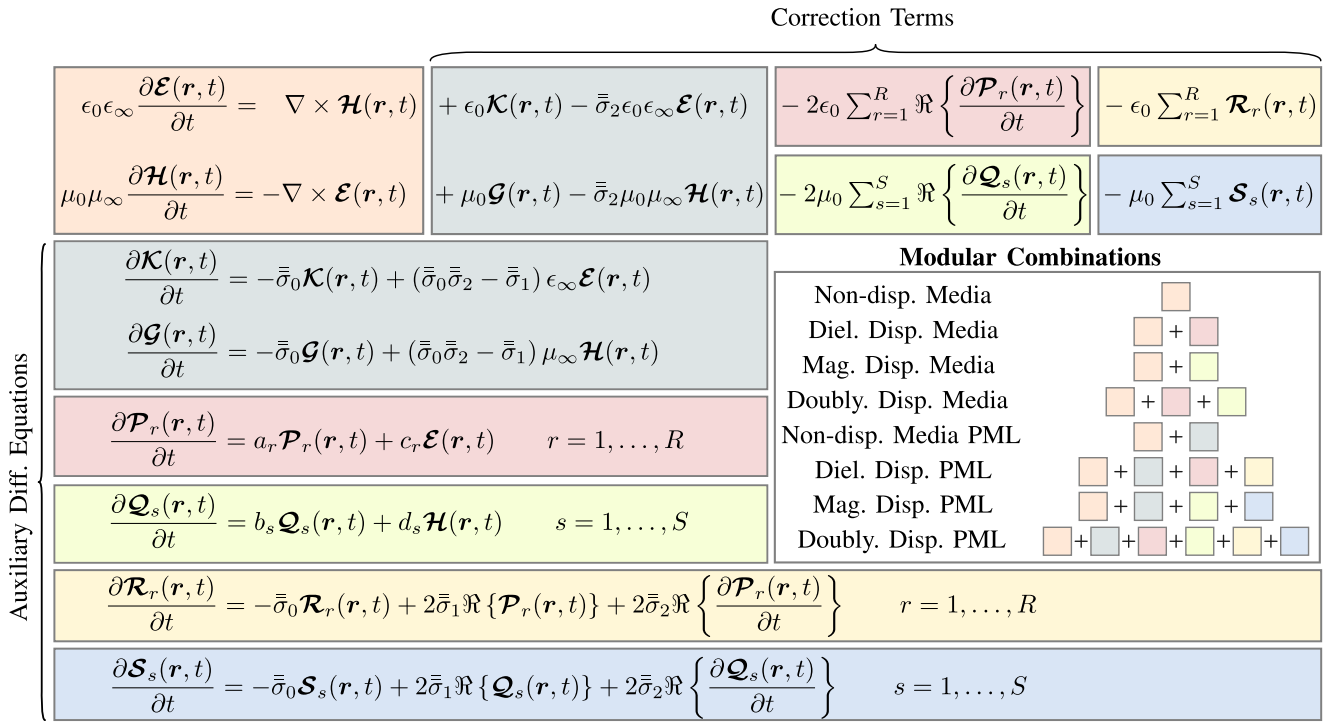

Fig. 1. Illustration of the modular implementation of Maxwell's equations containing doubly dispersive media truncated by PML.

$$
\begin{aligned}
&- \epsilon_0(\phi_h, \bar{\bar{\sigma}}_2\epsilon_\infty \boldsymbol{\mathcal{E}}_h)_{\Omega_h} \\
&- 2\epsilon_0 \sum_{r=1}^{R} \left(\phi_h, \Re\left\{\frac{\partial \boldsymbol{\mathcal{P}}_{h,r}}{\partial t}\right\}\right)_{\Omega_h} - \epsilon_0 \sum_{r=1}^{R} (\phi_h, \boldsymbol{\mathcal{R}}_{h,r})_{\Omega_h} \\
&+ \sum_{k=1}^{K} \left(\phi_h, \frac{-\hat{n}\times\eta_0\eta_\infty^+[\boldsymbol{\mathcal{H}}_h] + \hat{n}\times\hat{n}\times[\boldsymbol{\mathcal{E}}_h]}{2\{\{\eta_0\eta_\infty\}\}}\right)_{\partial\Omega_h^k} \qquad (3)
\end{aligned}
$$

$$
\begin{aligned}
\mu_0\left(\phi_h, \mu_\infty \frac{\partial \boldsymbol{\mathcal{H}}_h}{\partial t}\right)_{\Omega_h} &= (\phi_h, -\nabla\times\boldsymbol{\mathcal{E}}_h)_{\Omega_h} + \mu_0(\phi_h, \boldsymbol{\mathcal{G}}_h)_{\Omega_h} \\
&- \mu_0(\phi_h, \bar{\bar{\sigma}}_2\mu_\infty \boldsymbol{\mathcal{H}}_h)_{\Omega_h} \\
&- 2\mu_0 \sum_{s=1}^{S} \left(\phi_h, \Re\left\{\frac{\partial \boldsymbol{\mathcal{Q}}_{h,s}}{\partial t}\right\}\right)_{\Omega_h} - \mu_0 \sum_{s=1}^{S} (\phi_h, \boldsymbol{\mathcal{S}}_{h,s})_{\Omega_h} \\
&+ \sum_{k=1}^{K} \left(\phi_h, \frac{\{\{\eta_0\eta_\infty\}\}}{2}\left[\hat{n}\times\frac{[\boldsymbol{\mathcal{E}}_h]}{\eta_0\eta_\infty^+} + \hat{n}\times\hat{n}\times[\boldsymbol{\mathcal{H}}_h]\right]\right)_{\partial\Omega_h^k} \qquad (4)
\end{aligned}
$$

$$
\begin{aligned}
\left(\phi_h, \frac{\partial \boldsymbol{\mathcal{K}}_h}{\partial t}\right)_{\Omega_h} &= -(\phi_h, \bar{\bar{\sigma}}_0 \boldsymbol{\mathcal{K}}_h)_{\Omega_h} \\
&+ (\phi_h, (\bar{\bar{\sigma}}_0\bar{\bar{\sigma}}_2 - \bar{\bar{\sigma}}_1)\,\epsilon_\infty \boldsymbol{\mathcal{E}}_h)_{\Omega_h} \qquad (5)
\end{aligned}
$$

$$
\begin{aligned}
\left(\phi_h, \frac{\partial \boldsymbol{\mathcal{G}}_h}{\partial t}\right)_{\Omega_h} &= -(\phi_h, \bar{\bar{\sigma}}_0 \boldsymbol{\mathcal{G}}_h)_{\Omega_h} \\
&+ (\phi_h, (\bar{\bar{\sigma}}_0\bar{\bar{\sigma}}_2 - \bar{\bar{\sigma}}_1)\,\mu_\infty \boldsymbol{\mathcal{H}}_h)_{\Omega_h} \qquad (6)
\end{aligned}
$$

$$
\left(\phi_h, \frac{\partial \boldsymbol{\mathcal{P}}_{h,r}}{\partial t}\right)_{\Omega_h} = (\phi_h, a_r \boldsymbol{\mathcal{P}}_{h,r})_{\Omega_h} + (\phi_h, c_r \boldsymbol{\mathcal{E}}_h)_{\Omega_h} \qquad (7)
$$

$$
\left(\phi_h, \frac{\partial \boldsymbol{\mathcal{Q}}_{h,s}}{\partial t}\right)_{\Omega_h} = (\phi_h, b_s \boldsymbol{\mathcal{Q}}_{h,s})_{\Omega_h} + (\phi_h, d_s \boldsymbol{\mathcal{H}}_h)_{\Omega_h} \qquad (8)
$$

$$
\begin{aligned}
\left(\phi_h, \frac{\partial \boldsymbol{\mathcal{R}}_{h,r}}{\partial t}\right)_{\Omega_h} &= 2\left(\phi_h, \bar{\bar{\sigma}}_2 \Re\left\{\frac{\partial \boldsymbol{\mathcal{P}}_{h,r}}{\partial t}\right\}\right)_{\Omega_h} \\
&- (\phi_h, \bar{\bar{\sigma}}_0 \boldsymbol{\mathcal{R}}_{h,r})_{\Omega_h} + 2(\phi_h, \bar{\bar{\sigma}}_1 \Re\{\boldsymbol{\mathcal{P}}_{h,r}\})_{\Omega_h} \qquad (9)
\end{aligned}
$$

$$
\begin{aligned}
\left(\phi_h, \frac{\partial \boldsymbol{\mathcal{S}}_{h,s}}{\partial t}\right)_{\Omega_h} &= 2\left(\phi_h, \bar{\bar{\sigma}}_2 \Re\left\{\frac{\partial \boldsymbol{\mathcal{Q}}_{h,s}}{\partial t}\right\}\right)_{\Omega_h} \\
&- (\phi_h, \bar{\bar{\sigma}}_0 \boldsymbol{\mathcal{S}}_{h,s})_{\Omega_h} + 2(\phi_h, \bar{\bar{\sigma}}_1 \Re\{\boldsymbol{\mathcal{Q}}_{h,s}\})_{\Omega_h} \qquad (10)
\end{aligned}
$$

where $\boldsymbol{\mathcal{E}}_h, \boldsymbol{\mathcal{H}}_h, \boldsymbol{\mathcal{P}}_h, \boldsymbol{\mathcal{Q}}_h, \boldsymbol{\mathcal{R}}_h, \boldsymbol{\mathcal{S}}_h, \boldsymbol{\mathcal{G}}_h, \boldsymbol{\mathcal{K}}_h \in (V_h)^3$, and $\phi_h \in V_h$ with $V_h = \bigoplus_{k=1}^{K} P_N(\Omega^k)$ being the space of piecewise polynomial functions, $[q] = q^- - q^+$, $\{\{q\}\} = (q^- + q^+)/2$, and $\eta = \sqrt{\mu/\epsilon}$. Once the weak form is established, the solution can be obtained using the standard DGTD steps, as detailed in [4].

III. Numerical Results

The proposed formulation is validated by analyzing scattering problems assuming an incident transverse-magnetic (TM_z) plane wave given by

$$
\boldsymbol{\mathcal{E}}_{\text{inc}}(\boldsymbol{r}, t) = \hat{\boldsymbol{z}}\, g(t - \sqrt{\epsilon_0\mu_0}\,\hat{\boldsymbol{x}}\cdot\boldsymbol{r}) \qquad (11)
$$

$$
\boldsymbol{\mathcal{H}}_{\text{inc}}(\boldsymbol{r}, t) = \sqrt{\frac{\epsilon_0}{\mu_0}}\hat{\boldsymbol{x}} \times \boldsymbol{\mathcal{E}}_{\text{inc}}(\boldsymbol{r}, t) \qquad (12)
$$

with $g(t)$ being the cosine-modulated Gaussian waveform

$$
g(t) = \cos(2\pi f_c(t - t_0)) \exp\left(-(t - t_0)^2/\tau^2\right) \qquad (13)
$$

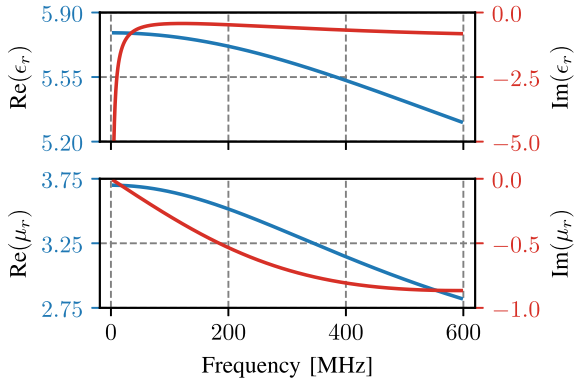

Fig. 2. Relative permittivity and relative permeability of the analyzed material.

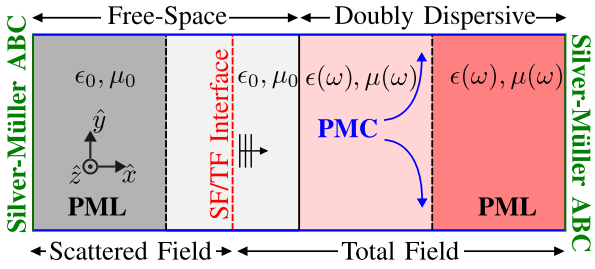

Fig. 3. Meridian cut view of the slab's 2-D validation case.

where f_c denotes the center frequency, τ characterizes the time constant, and t_0 represents a time delay. To analyze a frequency band from 100 MHz to 500 MHz, f_c was set to 300 MHz and τ was set to $1.25/f_c$ s. To ensure that the electromagnetic fields were zero at both the start and end of the simulation, a time delay t_0 of 7τ was applied, and the fields were simulated for a total duration of 20τ in all cases. The time step was chosen according to [4]. To model the dispersive media, we employed the doubly dispersive model, as described in [1], with relative permittivity and relative permeability responses, as shown in Fig. 2.

A second-degree polynomial defines the PML profile, with parameters chosen for normal incidence in vacuum to yield approximately 70 dB attenuation of the reflected wave.

The errors are analyzed using the relative L_2 error norm [3] and the normalized error, defined as $|\boldsymbol{\mathcal{E}}^n - \boldsymbol{\mathcal{E}}^a|/\boldsymbol{\mathcal{E}}_0$, where a refers to the analytical and n refers to the numerical values, and $\boldsymbol{\mathcal{E}}_0$ is the amplitude of the incident electric field.

A. Validation: Doubly Dispersive Slab

We first study the scattering of the TM_z plane wave by a doubly dispersive slab truncated by a doubly dispersive PML, as shown in Fig. 3.

The computational domain was sized at $3.0\lambda_c \times 2.0\lambda_c$, where λ_c is the wavelength at the center frequency f_c. The PML had a width of $0.5\lambda_c$, and the doubly dispersive slab was $1.0\lambda_c$ wide. The total-field scattered-field interface was positioned at the center of the scattered-field region, excluding the PML. To evaluate convergence, a coarse mesh with $1/6\lambda_c$ resolution (570 elements) and a refined mesh with $1/12\lambda_c$ resolution (2070 elements) were tested.

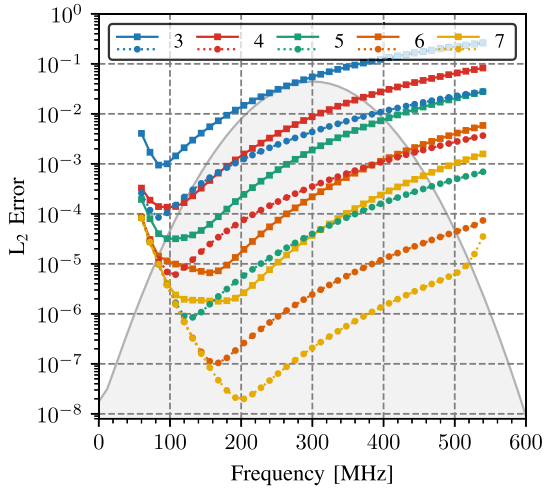

Fig. 4. L_2 error of the electric field varying the order of the elements. The gray area represents the frequency spectrum of the incident field.

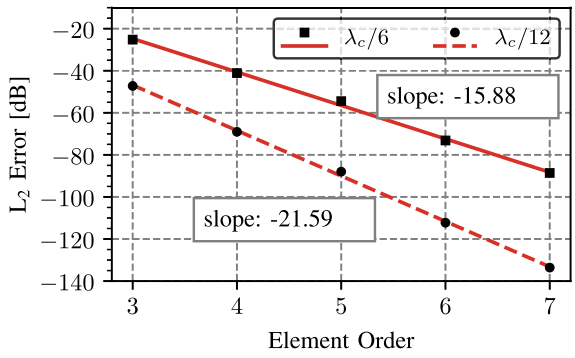

Fig. 5. Convergence rate of the L_2 error varying element orders at 300 MHz.

Fig. 4 shows the L_2 error compared to the analytical solution, whereas Fig. 5 shows the convergence of the solution with respect to the number of elements at 300 MHz. Compared to the results in [3], it is evident that using a static conductivity significantly increases and saturates the error at low frequencies, which was also observed in [22]. This occurs because the model employs the term $\sigma/(j\omega)$ [1], where the static conductivity σ leads to large contributions at low frequencies as ω approaches zero. In general, more complex doubly dispersive materials require both higher order schemes and denser meshes to achieve the same error levels as those observed in materials with only electric dispersion. Nevertheless, the convergence rate remains closely the same.

B. Doubly Dispersive Cylinder

To demonstrate the reduced modeling error achievable for curved objects, we analyze plane wave scattering by a doubly dispersive circular cylinder (see Fig. 6). Grids containing a few high-order curvilinear elements can achieve superior geometric accuracy compared to standard flat-faceted grids, improving high-fidelity simulation efficiency. However, these elements require complex integration (e.g., Gauss quadrature) over non-constant Jacobians and storage for element-specific operators, unlike the simpler calculations on standard linear elements.

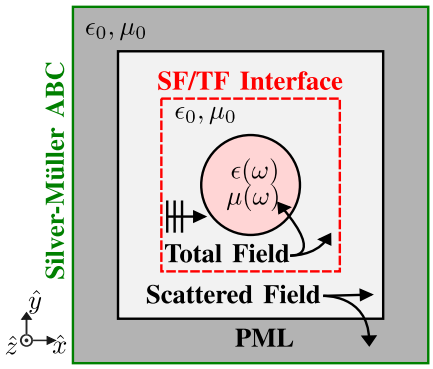

Fig. 6. Illustration of the cylinder's 2-D case study.

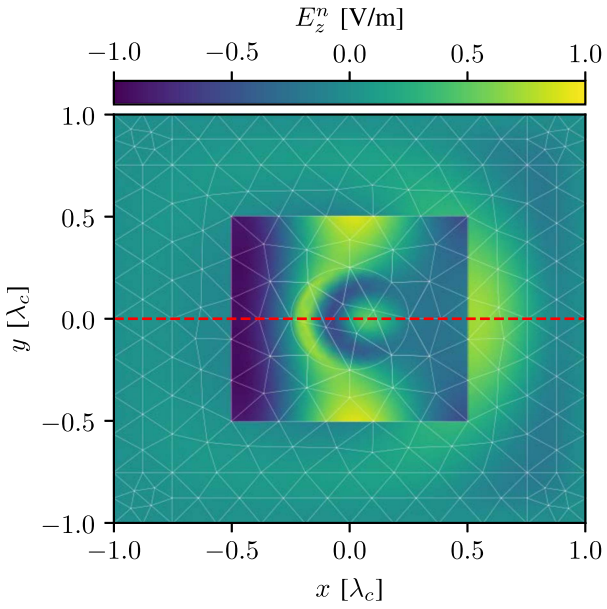

Fig. 7. Electric field at $t = 7\tau$ computed with fifth-order curvilinear DGTD.

TABLE I
STORAGE MEMORY AND TOTAL TIME COMPARISON

Method	Memory (MB)	Time (s)
Standard DGTD	2.29	21.12
Curv. DGTD	2.74	24.95

The computational domain has dimensions of $2.0\lambda_c \times 2.0\lambda_c$, with a PML width of $0.25\lambda_c$ and a cylinder radius of $0.25\lambda_c$. The performance of DGTD using fifth-order elements was compared for a mesh containing only standard linear elements versus one containing curvilinear elements at the boundary of the cylinder. Fig. 7 displays the electric field at $t = 7\tau$ obtained with the mesh containing curvilinear elements (374 elements and $1/10\lambda_c$ density). Fig. 8 plots the corresponding electric-field error at this time along the highlighted line $y = 0$.

The time-dependent error at the center of the cylinder is displayed in Fig. 9. The analytical time-domain solution was based on the frequency-domain series solution [23], as in [3], using 50 terms. A comparison of computational resources for the simulations is shown in Table I.

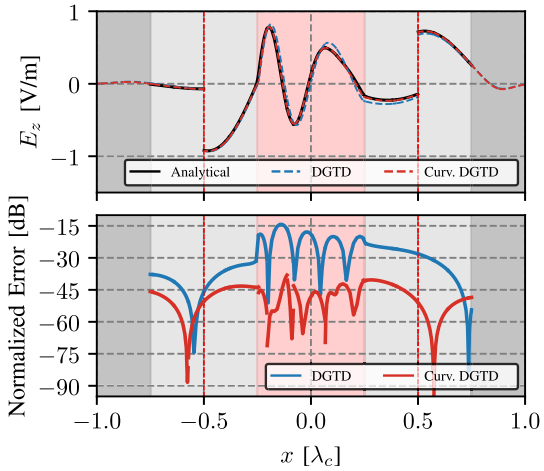

Fig. 8. Electric-field error profile along $y = 0$ at $t = 7\tau$.

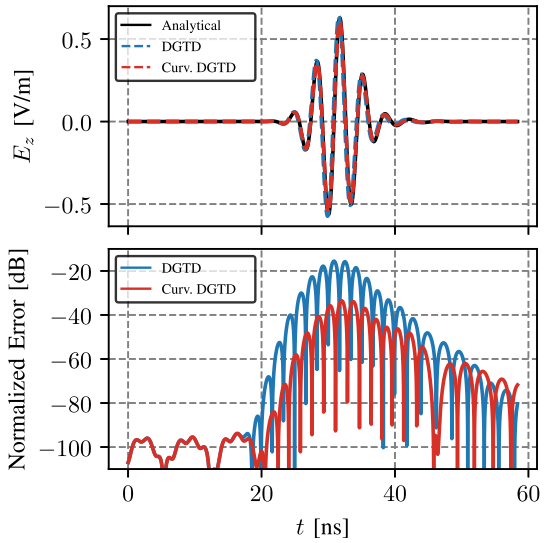

Fig. 9. Time evolution of the electric field at the cylinder center.

The results show that the curvilinear DGTD method achieves an error reduction of about 20 dB compared to the standard DGTD approach in this case. This improvement highlights the enhanced accuracy and efficiency of the proposed curvilinear DGTD method in modeling curved geometries while preserving computational performance. Notably, the computational cost of employing a small number of curvilinear elements is comparable to either doubling the mesh density or increasing the polynomial order by one degree across all elements.

IV. CONCLUSION

A modular DGTD algorithm was extended for modeling general doubly dispersive materials described by very general CCPR models. The modular implementation of the algorithm allows for the simulation of open domain problems by simply adding suitable correction terms that incorporate the PML absorbing boundary condition. The algorithm also integrates curvilinear elements to improve the accuracy over standard DGTD for modeling curved geometries without compromising the computational efficiency.

REFERENCES

[1] B. Donderici and F. L. Teixeira, "Mixed finite-element time-domain method for transient Maxwell equations in doubly dispersive media," *IEEE Trans. Microw. Theory Techn.*, vol. 56, no. 1, pp. 113–120, Jan. 2008.

[2] F. Chen, "A HIE-FDTD method for double-dispersive media," *IEEE Antennas Wireless Propag. Lett.*, vol. 23, no. 10, pp. 3023–3027, Oct. 2024.

[3] T. V. L. Amorim, E. J. Silva, F. J. S. Moreira, and F. L. Teixeira, "Modular discontinuous Galerkin time-domain method for general dispersive media with vector fitting," *IEEE Multiscale Multiphys. Comput. Techn.*, vol. 10, pp. 179–186, 2025.

[4] J. S. Hesthaven and T. Warburton, *Nodal Discontinuous Galerkin Methods*, vol. 54. New York, NY, USA: Springer, 2008.

[5] J. Lu, "An improved absorbing boundary condition for finite-element analysis," *IEEE Trans. Antennas Propag.*, vol. 72, no. 10, pp. 8109–8114, Oct. 2024.

[6] F. L. Teixeira, W. C. Chew, M. Straka, M. L. Oristaglio, and T. Wang, "Finite-difference time-domain simulation of ground penetrating radar on dispersive, inhomogeneous, and conductive soils," *IEEE Trans. Geosci. Remote Sens.*, vol. 36, no. 6, pp. 1928–1937, Nov. 1998.

[7] Y.-H. Chen, B.-Y. Wu, C.-Z. Yan, Z.-H. Zhao, and X.-Q. Sheng, "A discontinuous galerkin integral equation method for multiscale surface-wire structures," *IEEE Trans. Antennas Propag.*, vol. 72, no. 10, pp. 7883–7892, Oct. 2024.

[8] J.-P. Berenger, "A perfectly matched layer for the absorption of electromagnetic waves," *J. Comput. Phys.*, vol. 114, no. 2, pp. 185–200, 1994.

[9] T. Lu, W. Cai, and P. Zhang, "Discontinuous Galerkin time-domain method for GPR simulation in dispersive media," *IEEE Trans. Geosci. Remote Sens.*, vol. 43, no. 1, pp. 72–80, Jan. 2005.

[10] Y. Dong, M. Tang, P. Li, and J. Mao, "Transient electromagnetic-thermal simulation of dispersive media using DGTD method," *IEEE Trans. Electromagn. Compat.*, vol. 61, no. 4, pp. 1305–1313, Aug. 2019.

[11] Q. Yang, B. Wei, L. Li, R. Li, and D. Ge, "An SO-DGTD method of modeling dispersive media," *Waves Random Complex Media*, vol. 31, no. 2, pp. 389–402, 2021.

[12] X. Ji, W. Cai, and P. Zhang, "High-order DGTD methods for dispersive Maxwell's equations and modelling of silver nanowire coupling," *Int. J. Numer. Methods Eng.*, vol. 69, no. 2, pp. 308–325, 2007.

[13] M. R. Zunoubi, J. Payne, and W. P. Roach, "CUDA implementation of TE^z-FDTD solution of Maxwell's equations in dispersive media," *IEEE Antennas Wireless Propag. Lett.*, vol. 9, pp. 756–759, 2010.

[14] A. Akbarzadeh-Sharbaf and D. D. Giannacopoulos, "Finite-element time-domain solution of the vector wave equation in doubly dispersive media using Möbius transformation technique," *IEEE Trans. Antennas Propag.*, vol. 61, no. 8, pp. 4158–4166, Aug. 2013.

[15] J. Shibayama, K. Suzuki, T. Iwamoto, J. Yamauchi, and H. Nakano, "Dispersive contour-path FDTD algorithm for the Drude–Lorentz model," *IEEE Antennas Wireless Propag. Lett.*, vol. 19, no. 10, pp. 1699–1703, Oct. 2020.

[16] M. Han, R. W. Dutton, and S. Fan, "Model dispersive media in finite-difference time-domain method with complex-conjugate pole-residue pairs," *IEEE Microw. Wireless Compon. Lett.*, vol. 16, no. 3, pp. 119–121, Mar. 2006.

[17] H. Bao, L. Kang, S. D. Campbell, and D. H. Werner, "PML implementation in a nonconforming mixed-element DGTD method for periodic structure analysis," *IEEE Trans. Antennas Propag.*, vol. 67, no. 11, pp. 6979–6988, Nov. 2019.

[18] S. Lanteri, C. Scheid, and J. Viquerat, "Analysis of a generalized dispersive model coupled to a DGTD method with application to nanophotonics," *SIAM J. Sci. Comput.*, vol. 39, no. 3, pp. A831–A859, Jan. 2017.

[19] T. Zhang, H. Bao, D. Ding, and R. Chen, "Interior penalty DGTD method for solving wave equation in dispersive media described with GDM model," *IEEE Trans. Antennas Propag.*, vol. 69, no. 9, pp. 6105–6110, Sep. 2021.

[20] G. Xie et al., "Auxiliary differential equation (ADE) method based complying-divergence implicit FDTD method for simulating the general dispersive anisotropic material," *Opt. Exp.*, vol. 31, no. 11, May 2023, Art. no. 18468.

[21] G. Xie et al., "Extension of FLOD-FDTD method for multiterm modified Lorentz model," *IEEE Trans. Antennas Propag.*, vol. 71, no. 11, pp. 8830–8840, Nov. 2023.

[22] S. D. Gedney, J. C. Young, T. C. Kramer, and J. A. Roden, "A discontinuous Galerkin finite element time-domain method modeling of dispersive media," *IEEE Trans. Antennas Propag.*, vol. 60, no. 4, pp. 1969–1977, Apr. 2012.

[23] J.-M. Jin, *Theory and Computation of Electromagnetic Fields*, 2nd ed. Hoboken, NJ, USA: Wiley, Aug. 2015.